ISSN 0252-1075
Research Report No. RR-086

Contributions from
Indian Institute of Tropical Meteorology

ON STEP MOUNTAIN ETA MODEL

by

P. MOKHOPADHYAY,
S. S. VAIDYA,
J. SANJAY
and
S. S. SINGH

PUNE - 411 008
INDIA

OCTOBER 1999

CONTENTS

ON STEP MOUNTAIN ETA MODEL

P.Mukhopadhyay, S.S.Vaidya, J.Sanjay and S.S.Singh
Indian Institute of Tropical Meteorology, Pune-411008

1. Introduction

Since the begining of Numerical Weather Prediction technique, it has come a long way to reach the present day high resolution mesoscale modelling. The weather disturbances with a horizontal scale of 20 km to 200 km and temporal scale of a few minutes to 6 hour remained a major problem of NWP. The insufficient data network and unavailability of high resolution mesoscale model made it difficult to study meso-beta(20 to 200 km spatial dimension, few hour to 6 hour temporal dimension) and meso-gamma (2km to 20 km, a few minute to a few hour) systems. As a part of our on going effort in Forecasting Research Division to study the mesoscale systems, a high resolution mesoscale model is desirable. A version of high resolution ETA model, following Lazic et al (1990) is successfully implemented in IITM computer system. The model is run on a transformed spherical co-ordinate system which is a unique feature of the model. We prepared the schematic that helped us to visualize the spherical transformation. The model is run with NCMRWF analyses as the input for a case of monsoon depression from 25 July 1996 to 28 July 1996. The detail feature of the model co-ordinate, dynamics, physics, numerical methods and its application for the above mentioned case are being discussed here.

2. Eta Model

2.1 Problems of co-ordinate systems

The problems of co-ordinate surfaces in numerical modelling are related with the following factors.

a) Lower boundary condition due to presence of topography

b) Hydrostatic equation $$\frac{\partial \phi}{\partial p} = -\frac{RT}{p} \qquad (1)$$

c) horizontal pressure gradient term in momentum equation $$\frac{\partial \vec{v}}{\partial t} = ... - \nabla_p \phi + ... \qquad (2)$$

d) omega-alpha term in thermodynamic equation $$\frac{dT}{dt} = \frac{\kappa T \omega}{p} + ... \qquad (3)$$

In case the isobaric surfaces are cutting the lower boundary, problems will arise in solving the horizontal advection and diffusion terms. Pressure gradient force involves horizontal differencing of the geopotential at constant pressure surface. This discretization of the pressure gradient force will be related to the discretization of the hydrostatic equation.

If the constant co-ordinate surfaces intersect the lower boundary of the model, it will give rise to spurious solutions and this term due becomes a source of false energy generation (Mesinger et al 1988). As a step to solve this problem of lower boundary Phillips (1957) defined the sigma (σ) co-ordinate which unlike the pressure co-ordinate follow the bottom topography. Sigma is defined as $\sigma=\frac{p-p_T}{p_s-p_T}$, where p_s, p_T represent the pressure at the surface and top of the model domain respectively. The constant pressure surfaces and sigma surfaces above an idealistic elevated terrain are shown in fig 1. Problem in sigma co-ordinate lies in the calculation of pressure gradient force and dealing hydrostatic equation near mountainous region. Pressure gradient force term in sigma co-ordiante takes the following form $-\bar{\nabla}_p\phi=-\bar{\nabla}_\sigma\phi-RT\bar{\nabla}_\sigma \ln p_s$ (4)

where $\bar{\nabla}_p$ & $\bar{\nabla}_\sigma$ are the horizontal differential vector operators in a constant pressure and constant sigma surfaces respectively. Over steep terrain these two terms on the right hand side of equation (4) tend to be large in absolute values and have opposite signs. If for example, they are individually ten times greater than their sum, 1% error in temperature will result a 10% error in pressure gradient force (Sundqvist 1975). Thus this term becomes a spurious source of generating erroneous pressure gradient force.

The hydrostatic equation in sigma co-ordinate can be written as $\frac{\partial\phi}{\partial\sigma}=-\frac{RT}{\sigma}$ (5)

The difference form of equation (5) will be $\Delta\phi_k=-RT_k\Delta\ln\sigma_k$ (6)

where $\Delta T_k=T_{k+\frac{1}{2}}-T_{k-\frac{1}{2}}$

$$T_k=\frac{1}{2}\left[T_{k-\frac{1}{2}}+T_{k+\frac{1}{2}}\right]$$

To maintain hydrostatic consistency the required condition is $\left|\delta_x\phi\right|_\sigma\Delta x\le\left|\delta_\sigma\phi\right|\Delta\sigma$ (7)

this constraint will be violated near mountainous region as shown in fig 2.

Eta co-ordinate was introduced by Fedor Mesinger (1984) in order to reduce the error mainly arising from the pressure gradient force term near steep terrain.
Eta co-ordinate is defined by the following equation.

$$\eta=\underbrace{\left(\frac{p-p_T}{p_{sfc}-p_T}\right)}_{\sigma}\underbrace{\left[\frac{p_{ref}(z_{sfc})-p_T}{p_{ref}(0)-p_T}\right]}_{\eta_s} \quad (8)$$

$$\eta=\sigma\eta_s$$

where reference atmosphere is defined as follows

Mean sea level pressure = $p_{ref}(0)$ = 1013.25 hPa

Temperature = T= 288.15 K

G = 9.8 m/s^2

R= 287.04 J/K.kg

Pressure at the top of the domain = p_T

$$p_{ref}(z) = p_{ref}(0)\exp\left(-gz/RT\right) \tag{9}$$

z_{sfc} = Height of the elevated model lower boundary due to topography with respect to mean sea level (msl). Schematic diagram in fig 3 is drawn to explain the quasi horizontal nature of constant Eta surfaces. Two points P1 and P2 are considered. They are lying nearly at the same height above mean sea level (msl) but at different sigma levels σ_1 and σ_2. The pressure at surface below points p_1 and p_2 are p_{sfc1} & p_{sfc2} respectively and pressure at points p_1 and p_2 are p_{p_1} & p_{p_2}.

As p_1 and p_2 are almost on the same height, So $p_{p_1} - p_T \approx p_{p_2} - p_T$

But pressure at the surface below point p_1 and p_2 are different.

Hence $p_{sfc2} - p_T > p_{sfc1} - p_T$ and $\sigma_2 < \sigma_1$

This difference is reduced by multiplying the sigma expression by a normalising factor F. Factor F is defined as

$$F = \frac{p_{ref}(0) - p_T}{p_{ref}(z_{sfc}) - p_T}$$

At point P_1, value of F is F_{P_1} and value of F at P_2 is F_{P_2}. It can be seen from fig 3 that $F_{P_1} < F_{P_2}$ that is $\frac{1}{F_{P_1}} > \frac{1}{F_{P_2}}$, Therefore $\frac{\sigma_2}{F_{P_2}} \approx \frac{\sigma_1}{F_{P_1}}$

This explains the reason behind the eta surfaces becoming quasi horizontal unlike sigma surfaces.

2.2 Horizontal Transformation

In order to achieve higher computational efficiency of the model code, a transformed latitude - longitude co-ordinate system is used. This system is obtained by rotation of the natural geodetic latitude - longitude in such a way that the intersection of the equator and zeroth meridian of the transformed system provides a more uniform horizontal grid spacing by reducing the meridional convergence significantly. The detail schematic of co-ordinate transformation is shown in fig 4. This schematic clearly depicts the rotational transformation

that is applied in the model. This transformation adds to the stability of the model as Δx will have lesser reduction in this set up. This transformation helps in choosing larger time step for the model time integration. Fig 4. represents the geodetic latitude and longitude (ϕ,λ) of a point and transformed latitude and longitude are represented by (Φ,Λ). At the centre of the domain ϕ,λ, and Φ,Λ are prescribed as follows

$$\phi=\phi_0\ ,\ \lambda=\lambda_0\ ,\ \Phi=0\ ,\ \Lambda=0$$

With these notations, the relations between the transformed latitude - longitude and geodetic latitude-longitude is written as follows

$$\Phi=\tan^{-1}\left(\frac{z}{\sqrt{x^2+y^2}}\right)$$

$$\Lambda=\tan^{-1}\left(\frac{y}{x}\right)$$

$$x=\cos\phi_0\cos\phi\cos(\lambda-\lambda_0)+\sin\phi_0\sin\phi$$
$$y=-\cos\phi\sin(\lambda-\lambda_0)$$
$$z=-\sin\phi_0\cos\phi\cos(\lambda-\lambda_0)+\cos\phi_0\sin\phi$$
$$\phi=\sin^{-1}(\sin\Phi\cos\phi_0+\cos\Phi\sin\phi_0\cos\Lambda)$$
$$\lambda=\lambda_0\pm\cos^{-1}\left[\frac{\cos\Phi\cos\Lambda}{\cos\phi\cos\phi_0}-\tan\phi\tan\phi_0\right]$$

The schematic diagram of the size of the domain before and after the transformation is shown in fig 5.

2.3 Basic equations in Eta co-ordinate.

The basic prognostic variables are surface pressure, temperature, specific humidity, wind velocity (u,v). The basic equations in eta co-ordinate can be written as follows.

$$\frac{\partial}{\partial t}\left(\frac{\partial p}{\partial\eta}\vec{V}\right)+\vec{\nabla}_\eta\left(\frac{\partial p}{\partial\eta}\vec{V}\vec{V}\right)+\frac{\partial}{\partial\eta}\left(\frac{\partial p}{\partial\eta}\eta\vec{V}\right)+\frac{\partial}{\partial\eta}\left[f\hat{k}\,x\vec{V}+\nabla_\eta\phi+\frac{R_dT}{p}\vec{\nabla}_\eta p+\vec{F}\right]=0$$

$$\frac{dT}{dt}+\frac{\kappa T\omega}{p}+T'+\frac{g}{c_p}\frac{\frac{\partial R}{\partial\eta}}{\frac{\partial p}{\partial\eta}}=0$$

$$\frac{\partial\phi}{\partial\eta}=-\frac{R_dT_v}{p}\frac{\partial p}{\partial\eta}$$

$$\frac{\partial p_s}{\partial t} = -\int_0^{\eta_s} \vec{\nabla}_\eta \cdot \left[\frac{\partial p}{\partial \eta}\vec{V}\right] d\eta$$

$$\frac{1}{\eta_s}\frac{\partial p_s}{\partial t} + \vec{\nabla}_\eta\left[\frac{\partial p}{\partial \eta}\vec{V}\right] + \frac{\partial}{\partial \eta}\left(\frac{\partial p}{\partial \eta}\dot{\eta}\right) = 0$$

$$\omega \equiv \frac{dp}{dt} = \int_0^{\eta} \vec{\nabla}\left(\vec{V}\frac{\partial p}{\partial \eta}\right) d\eta + \vec{V}.\nabla p$$

$$\frac{\partial p}{\partial \eta} = \frac{p_s - p_T}{\eta_s}$$

$$\dot{\eta}\frac{\partial p}{\partial \eta} = -\frac{\eta}{\eta_s}\frac{\partial p_s}{\partial t} - \int_0^{\eta} \vec{\nabla}_\eta\left(\frac{\partial p}{\partial \eta}\vec{V}\right) d\eta$$

$$\frac{dq}{dt} + q' = S$$

Where F = frictional and turbulent effects on the velocity
q' = turbulent effect on specific humidity
ϕ = geopotential
T' = turbulent effects on temperature
R = net vertical radiative flux
S = source and sinks of water vapour

Other symbols are having conventional meaning.

2.4 Horizontal and vertical structure

So far as the horizontal grid is concerned, model has used ***Arakawa E*** type staggering. The horizontal grid size chosen for the study is 0.5 deg x 0.5 deg. The staggered grid with scalar and vector points are shown in fig 6. The points denoted by **h** carry surface pressure, temperature, specific humidity, cloud water, vertical velocity, turbulent kinetic energy. The **V** points carry u, v components of the horizontal wind. In the simulation of geostrophic adjustment process B/E grid shows grid separation problem at short wave length. A method which largely eliminates this problem has been used in the model (Mesinger, 1973; Janjic, 1979). E grid is preferred over C grid as the later displays significant error for higher internal mode at all wave lengths in the geostrophic adjustment process. Lastly the linear amplitude response to forcing by topography in the B and E grid is more accurate than C grid schemes (Dragasovac et al , 1987).

The schematic diagram of the eta levels and vertical staggering of the variables are shown in fig 7. There are thirty-two vertical eta levels. The pressure at the top of the model domain is 10 hPa. The prognostic variables are vertically staggered. The temperature (T), specific humidity (q) and horizontal wind components (u,v) are located in the middle of vertical layers (half level), while the vertical velocity ($\dot{\eta}$) and geopotential (ϕ) are placed at the interfaces (full levels) of the layers.

2.5 Silhouette Mountains

The US navy 10' x 10' topography is used to construct silhouette topography. The silhouette averaging of the US navy data consists of following steps.

a) Group of four adjacent height points are considered

b) Each of the square grid boxes is divided into four subboxes.

c) Actual surface elevations at a resolution of 10' x 10' in each subbox are read from US navy data set. Mean is found within each subbox. These means are denoted by **z** in fig 6. Maximum elevation along each row and column are determined by **S** and is shown in fig 6. The maxima are calculated as follows

$$S1 = \max(z1,z2,z3,z4)$$
$$S2 = \max(z5,z6,z7,z8)$$
$$\cdots\cdots\cdots\cdots$$
$$S8 = \max(z4,z8,z12,z16)$$
$$\text{Silhouette height} = \frac{1}{8}\sum_{i=1}^{8} S_i$$

After the construction of silhouette mountain, the steps are calculated. This step mountain is finally used in the model. The construction of step mountain from silhouette is being done as follows

a) Firstly the heights of the eta levels with respect to reference atmosphere are calculated.

b) The silhouette height is rounded to the nearest possible eta level height. The steps chosen for constructing the model mountain are 0.14, 0.30, 0.48, 0.68, 0.89, 1.13, 1.39, 1.67, 1.97, 2.29, 2.64, 3.01, 3.4, 3.83, 4.28, 4.76, 5.27, 5.82 Km

This gives rise to the step like mountain which is shown in fig 8 for Indian region.

2.6 Top and bottom boundary condition

From equation (8) it can be shown that

$$\eta=0 \quad \text{at} \quad p=p_T$$

$$\eta=1 \quad \text{at} \quad z=z_{sfc}=0$$

$$\eta=\eta_s \text{ at } z=z_{sfc}$$

Top and bottom boundary conditions for vertical velocity are as follows.

$$\dot{\eta}=0 \text{ at } \eta = 0$$

$$\dot{\eta}=0 \text{ at } \eta = \eta_s = 1$$

2.7 Horizontal boundary condition

The tendencies of the forecast quantities are obtained by assuming linear change during each twelve hour period and are applied to the outer rows after every adjustment time step (60 secs) during the integration. After each update of the outer row, the wind components normal to the boundary are checked except the eight (boxed) velocity points nearest the four corners. If the normal component is outward, the tangential component is replaced by a linear extrapolation of the first two similar components inside the integration domain.
The second row within the outer boundary is a blend of outer row and third row inside which is included in integration. The quantities PD (pressure difference between the surface and top of domain), T and q are updated each Δt (60 secs) at the scalar points of the second row by four point averaging,

$$T(1,2) = 1/4[T(1,1) + T(2,1) + T(1,3) + T(2,3)]$$

Wind components are updated by same four point averaging at all points except four circled velocity points (fig 9) where a six point weighted average is chosen.

u(2,2)=4/15[u(1,1) + u(2,1) + u((2,3)] + 1/15[u(1,2) + u(1,4) + u(2,4)]

.....

u(IM-1,2)=4/15[u(IM-1,1) + u(IM-2,1) + u(IM-2,3)] + 1/15[u(IM,2) + u(IM,4) + u(IM-1,4)]

In the inside boundary along the vertical wall of the step mountain no slip boundary condition is chosen. The submerged velocity points below the model mountain are put to be zero.

2.8 Time difference technique

The eta model employs forward-backward scheme modified to prevent gravity wave

separation(Mesinger, 1973 ; Janjic, 1979)

$$u^{n+1} = u^n - \Delta t_{adj} P_x^{n+1}$$

$$v^{n+1} = v^n - \Delta t_{adj} P_y^{n+1}$$

$$PD^{n+1} = PD^n - \left[\sum_{L=1}^{LM} \vec{\nabla}_\eta \cdot \frac{\partial p}{\partial \eta} \vec{V} \Delta \eta \right]^n$$

P_x, P_y = Components of pressure gradient force

LM = Lowest predictive level above the surface

PD = Difference of surface pressure and pressure at top of domain

Mass field is determined using a forward time differencing while velocity components are obtained using a backward time difference. New values of PD are determined first then wind components are updated using the pressure gradients of the new mass field.
The Coriolis and curvature terms are added in the following way

$$u^{n+1} = u^n + f^n \Delta t_{adj}\left[\frac{v^{n+1} + v^n}{2}\right] - \Delta t_{adj} P_x^{n+1}$$

$$v^{n+1} = v^n + f^n \Delta t_{adj}\left[\frac{u^{n+1} + u^n}{2}\right] - \Delta t_{adj} P_y^{n+1}$$

For vertical advection of the temperature, specific humidity, turbulent kinetic energy and horizontal momentum, the Euler backward scheme (Matsuno) is used. With this scheme, a first step is made using the Euler scheme to produce a preliminary forward guess.

$$A^{n+1} = A^n - \Delta t\left(\dot{\eta}\frac{\partial A}{\partial \eta}\right)^n$$

The approximation A^{n+1} is then used to make the backward step.

Scheme is explicit and of first order accuracy.
For horizontal momentum advection, a forward then centred time differencing scheme is used which is unconditionally stable. Using Euler scheme, first a forward guess is produced at half of the integration time step.

$$v^{n+\frac{1}{2}} = v^n - \frac{\Delta t}{2}\left(v.\vec{\nabla}v\right)^n$$

Such calculated forward guess is then used to obtain the final value

$$v^{n+1} = v^n - \Delta t\left(v.\vec{\nabla}v\right)^{n+\frac{1}{2}}$$

For horizontal advection of the other model variables, the same scheme is used with the forward step $\sqrt{2}/2$ times the advection time step for momentum equation

$$v^{n+\frac{\sqrt{2}}{2}} = v^n - \frac{\sqrt{2}}{2}\Delta t\left(v.\vec{\nabla}v\right)^n$$

this value is used to calculate the final value.

$$v^{n+1} = v^n - \Delta t\left(v \cdot \bar{\nabla} v\right)^{n+\frac{\sqrt{2}}{2}}$$

A time splitting technique is applied in order to achieve higher computational efficiency of the model. The advection time step is chosen as twice as longer than adjustment time step Contrbution for the remaining physical forcing terms (turbulence, convection, radiation) is calculated using time step n times longer than the time step for adjustment.

3.Physics of the Eta model

The eta models physical package describes turbulent exchange, large scale and convective precipitation, lateral diffusion, surface processes and radiation.

3.1 Turbulent Exchange

The process of turbulent transfer is described in the eta model by applying Mellor-Yamada closure theory (Mellor et al, 1974, 1982) which yields exchange coefficients used to calculate the heat, moisture and momentum exchange through model layer interfaces. The level 2.5 closure theory in Mellor-Yamada hierarchy is used for PBL and free atmosphere. This scheme is chosen for computational efficiency. Level 2 turbulent closure in the Mellor-Yamada hierarchy is chosen for surface layer.

3.2 Moist processes

Large scale precipitation : Large scale precipitation is calculated with the assumption that condensation occurs if the relative humidity is greater than the threshold (RH = 95%)

Convective processes : Shallow and deep convection scheme of Betts (1986) and Betts et al (1986) over land and ocean are used in the model.

3.3 Surface processes

The Oregon State University (OSU) scheme for parameterization of surface processes is used in the eta model. Approximate thermal balance is assumed to be existing in the surface ground layer and is expressed by a prognostic temperature equation. Single bucket model is used for surface hydrology.

3.4 Radiation

GFDL radiation parameterization scheme is used for short wave and long wave solar radiation in the eta model

4. Data used

A case of active monsoon situation with a monsoon depression formed over Head Bay of Bengal and moved in a northwesterly direction is chosen for this study.

The daily global analyses at 1.5° provided by the GDAS, NCMRWF are bilinearly interpolated to the eta model rotated grid and used as input. The surface fields of sea surface temperature (SST), albedo and ground wetness are used from monthly climatology.

5. Results

Mean sea level pressure

Twenty four, forty eight and seventy two hour forecast of mean sea level (msl) pressure from eta model with horizontal resolution of 0.5 ° along with the corresponding analysis are shown in fig 10. The intensity of the depression predicted by the model is found to be stronger than that seen in the corresponding analysis. The innermost isobar in the 24 hour forecast and 48 hour forecast are 990 hPa and 992 hPa respectively as against 992 hPa and 996 hPa of 26 July 27 July analysis. The depression shows weakening in the third day forecast but the number of closed isobars and innermost isobar show stronger intensity than what is seen in 28 July analysis. The location of the centre of the depression is found to be south of the verification analysis. The pressure gradient in the west coast is found to be intense in forecasted msl pressure diagram. So as far as msl pressure is concerned it is found that eta model is able to reproduce the typical active monsoon pattern but the system is forecasted south of that seen in corresponding analysis and the intensity is found to be stronger in predicted msl pressure field.

Streamlines and isotachs

The forecast and corresponding analysis of 850 hPa streamlines and isotachs for 26 July, 27 July and 28 July are shown in fig 11. The low level jet typical to the active monsoon regime is found to be 20 m/s in the analysis. The corresponding forecast also shows the maxima of wind to be 20 m/s but covering a wider region in the Arabian Sea with respect to that of the

analysis. The streamlines also suggest that the centre of the system is shifted southwards in the predicted diagrams and movement is found to be slower.

Specific humidity

The distribution of specific humidity at 850 hPa as predicted by the model and seen in the analysis are shown in fig 12. The distribution of specific humidity in 24, 48 and 72 hour forecast shows a gradient along the monsoon trough region . The maximum is found to be near the south east end of monsoon trough and minima is lying near the north west end of monsoon trough. The contour of specific humidity is showing a shift along with the movement of the depression.

Temperature

The forecast and analysed isotherm at 500 hPa are shown in fig 13. The forecast is found to be noisier. The model has predicted a stronger heat low with the innermost isotherm showing 276 K as compared to 274 K seen in the analysis. The temperature gradient from north to south along the latitude is correctly reproduced.

Rainfall

The eta model predicted rainfall for Day 1, Day 2, Day 3, are shown in fig 14. The figure clearly shows that the model is able to reproduce the rainfall zones in association with the monsoon depression and in association with the off shore trough along west coast. The rainfall zone shifted northwest ward with movement of the depression. The heavy rainfall in the windward side of the western ghat hills are also properly reproduced.

6. Summary

i) With this attempt eta model is first time implemented over tropical region like India.
ii) The model has some unique features. It does not require any map projection and can be run in equal latitude longitude grid with transformed grid. The schematic of the rotational transformation first time prepared and presented here clearly depicts this feature.
iii) As a first attempt to study the performance of eta model over Indian region, it is seen that the model is able to reproduce satisfactorily the synoptic features and rainfall patterns of the monsoon depression considered here. The model has correctly predicted the south west sector of the depression to be the region of maximum rainfall activity.
iv) Eta model also predicts correctly the heavy rainfall zones in the wind ward side of the Western Ghat hills and rain shadow zones in the lee side of the mountain.
v) In future the model will be run at a higher resolutions to study its capability to simulate the heavy localised rainfall over Indian region.

Acknowledgement

The authors are thankful to Dr. G.B.Pant, Director, IITM for his interest in the study. They gratefully acknowledge Dr. Lazar Lazic of Belgrade University for providing the model code. The first author is thankful to Dr. Fedor mesinger, NCEP for his suggestions and comments in implementing ETA model over Indian region. The grid point analyses is provided by NCMRWF and the rainfall data is provided by IMD. Authors acknowledge Brian Dotty for using Grads software for plotting diagrams.

References .

Arakawa, A., 1972 : Design of the UCLA general circulation model. Numerical Simulation of Weather and Climate. Dept. of Meteorology, Univ. of California, Los Angeles, Tech. Rept. No. 7, 116 pp.

Arakawa, A, and V.R. Lamb, 1981 : A potential enstrophy and energy conserving scheme for the shallow water equations. *Mon. Wea. Rev.*, 109, 18-30.

Betts, A.K., 1986 : A new convective adjustment scheme. Part I : Observational and Theoretical basis. *Quart. J. Roy. Meteor. Soc.*, 112, 677-691.

Betts, A.K., and M.J. Miller, 1986 : A new convective adjustment scheme. Part II : Single column tests using GATE wave, BOMEX, ATEX and Arctic air mass data sets. *Quart. J. Roy. Meteor. Soc.*, 112, 693-709.

Black, T.L., 1988 : The step-mountain eta co-ordinate regional model : A documentation. NOAA/NWS/NMC Washington, 47 pp.

Davies, R., 1982 : Documentation of the solar radiation parameterization in the GLAS climate model. NASA Tech. Memo. 93961, 57 pp.

Deardorff, J., 1978 : Efficient prediction of ground temperature and moisture with inclusion of a layer of vegetation. *J. Geophys. Res.* 83, 1989-1903.

Janjic, Z. I., 1974 : A stable centred difference scheme free of two grid-interval noise. *Mon.Wea. Rev.*, 102, 319-323.

Janjic, Z. I., 1979 : Forward-backward scheme modified to prevent two grid interval noise and its application in sigma co-ordinate models. *Contrib. Atmos. Phys.*, 52, 69-84.

Janjic, Z. I., 1954 : Non-linear advection schemes and energy cascade on semi-staggered grids. *Mon.Wea.Rev.*, 112, 1234-1245.

Janjic, Z. I., 1990 : The step-mountain co-ordinate : Physical package. *Mon.Wea. Rev.*, 118, 1429-1443.

Janjic, Z. I., 1994 : The step-mountain Eta co-ordinate model : Further developments of the convection, viscous sub-layer and turbulence closure schemes, *Mon.Wea.Rev.*, 122, 927-945

Janjic, Z. I., and A. Wiin-Nielsen, 1977 : On geostrophic adjustment and numerical procedures in a rotating fluid. *J. Atmos. Sci.*, 34, 297-310.

Janjic, Z. I., and F. Mesinger, 1989 : Response to small scale forcing on two staggered grids used in finite difference models of the atmosphere. *Quart. J. Roy. Meteor. Soc.*, 115, 1167-1176.

Janjic, Z. I., F. Mesinger, and T.L. Black, 1995 : The pressure advection term and additive splitting in split-explicit models. *Quart. J. Roy. Meteor. Soc.*, 121, 953-957.

Lazic, L. and B. Telenta, 1990 : Documentation of the UB/NMC Eta model. Tropical Meteorology Research Programme,WMO, Geneva,WMO/TD No. 360, 204 pp.

Liu, W.T., K.B. Katsares and J.A. Businger, 1979 : Bulk parameterization of air sea exchanges of heat and water vapour including the molecular constraints at the interface. *J. Atmos. Sci.*, 36, 1722-1735.

Labocki, L., 1993 : A procedure for the derivation of surface-layer bulk relationships from simplified second order closure models. *J. Appl. Meteor.*, 32, 126-138.

Mellor, G.L. and T. Yamada, 1974 : A hierarchy of turbulence closure models for planetary boundary layers. *J. Atmos. Sci.*, 31, 1791-1806.

Mesinger, F., 1973 : A method for construction of second order accuracy difference schemes permitting no false two-grid-interval wave in the height field. *Tellus*, 25, 444-458.

Mesinger, F., 1977 : Forward-backward scheme and its use in a limited area model. *Contrib. Atmos. Phys.*, 50, 200-210.

Mesinger, F., 1985 : Problems and Numerical Methods of the Incorporation of Mountains in Atmospheric Models. *Lect.App.Math*, 22, 1985

Mesinger, F, and A. Arakawa, 1976 : Numerical methods used in Atmospheric models. Vol. 1, GARP Publication Series No. 17, WMO, Geneva, 64 pp.

Mesinger, F, Z.I. Janjic, S. Nickovic, D. Gavrilov and D.G. Deaven, 1988 : The step mountain co-ordinate : model description and performance for cases of Alpine lee cyclogenesis and for a case of an Appalachian redevelopment. *Mon.Wea.Rev.*, 116, 1493-1518.

Miyakoda, K., and J. Sirutis, 1984 : Manual of the E-Physics. GFDL/NOAA Tec. Note, 68 pp.

Monin, A.S., and A.M. Obukhov, 1954 : Basic laws of turbulent mixing in the surface layer of the atmosphere. *Contrib. Geophys. Inst. Acad. Sci.*, USSR, 151, 163-187.

Phillips, N.A., 1957 : A co-ordinate system having some special advantages for numerical forecasting. *J. Meteor.*, 14, 184-185

Smagorinsky, J., 1963 : General Circulation experiments with the primitive equations. Part I: The basic experiment. *Mon.Wea. Rev.*, 91, 99-164.

Vasiljevic, D., 1982 : The effect of Mesinger's procedure for preventing grid separation on the geostrophic mode. *Contrib. Atmos. Phys.*, 55, 177-181.

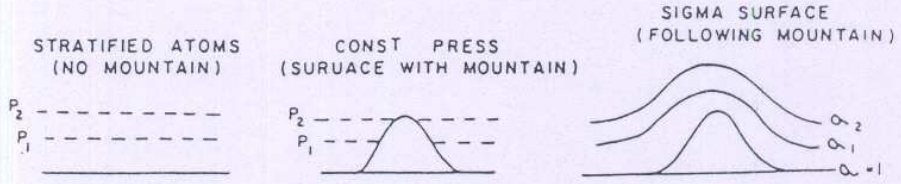

fig 1 : Pressure and sigma levels over an elevated surface

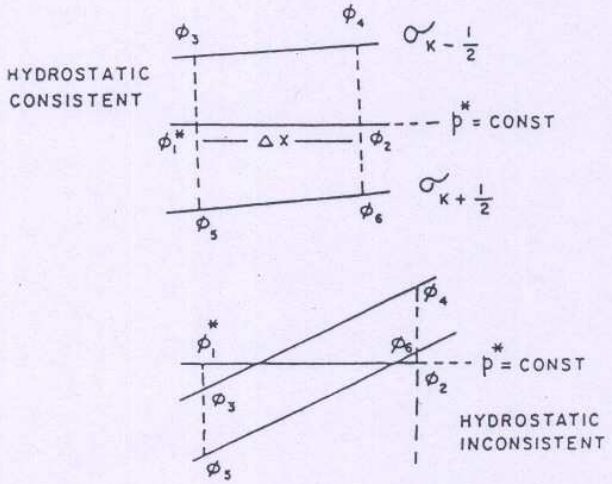

fig 2 : Constant sigma surface over steep terrain

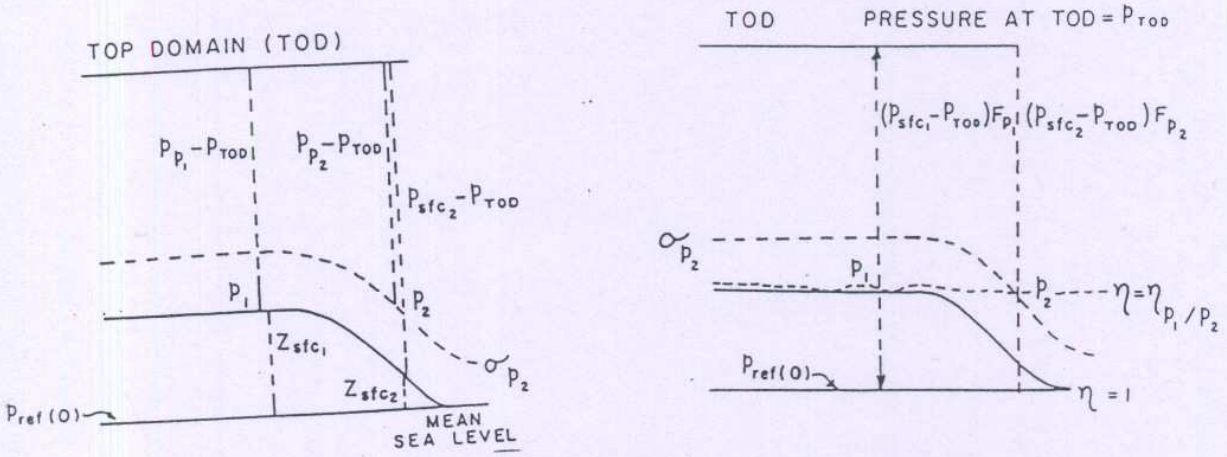

p_{p1} = Press at P_1

p_{p2} = Press at P_2

p_{sfc1} = Surface press at P_1

p_{sfc2} = Surface press at P_2

$p_{p1} - p_{TOD} \approx P_{p2} - p_{TOD}$

BUT

$P_{sfc1} - P_{TOD} < P_{sfc2} - P_{TOD}$

Therefore $\sigma_{p1} > \sigma_{p2}$

$$F = \frac{p_{ref}^{(0)} - p_{TOD}}{p_{ref}(Zsfc) - p_{TOD}}$$

$F_{P1} > F_{P2}$

fig 3 : Constant Eta and Sigma surface (T.L.Black 1994)

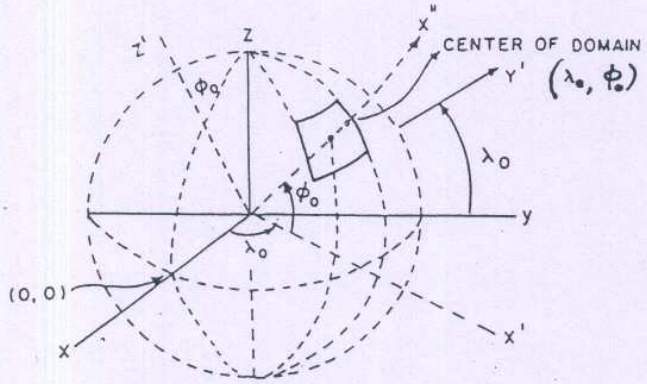

Before Rotation : x, y, z

After Rotation : x", y', z'

fig 4 : Spherical transformation of co-ordinate axes

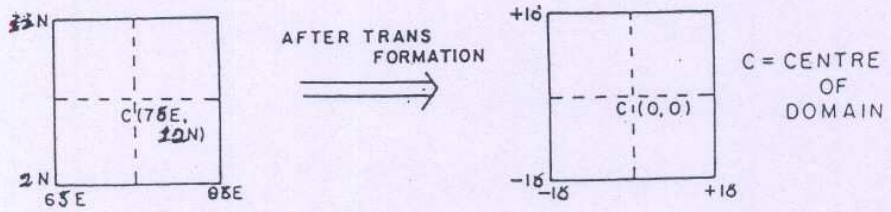

fig 5 : Selected domain before and after the tranformation

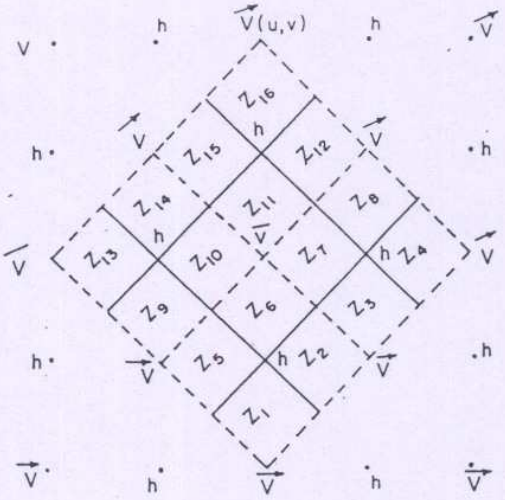

fig 6 : Vector and scalar points in staggered E-grid

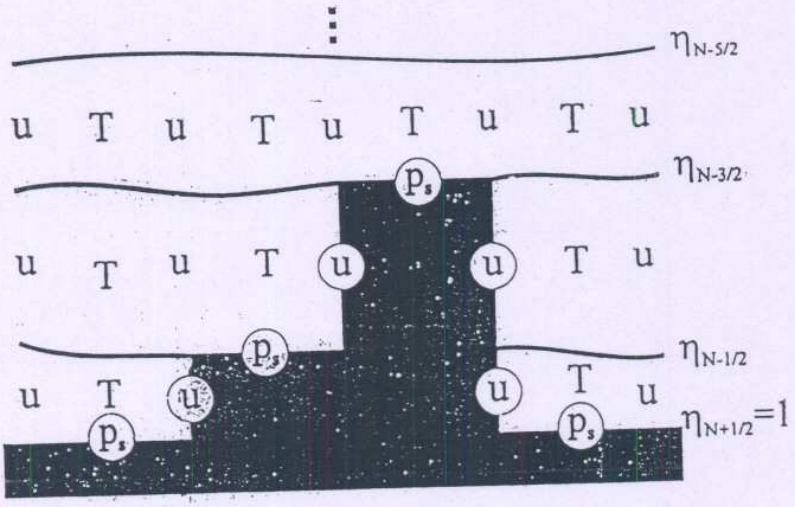

fig 7 The eta vertical coordinate system and distribution of the mo variables in the vertical (Mesinger et al, 1988)

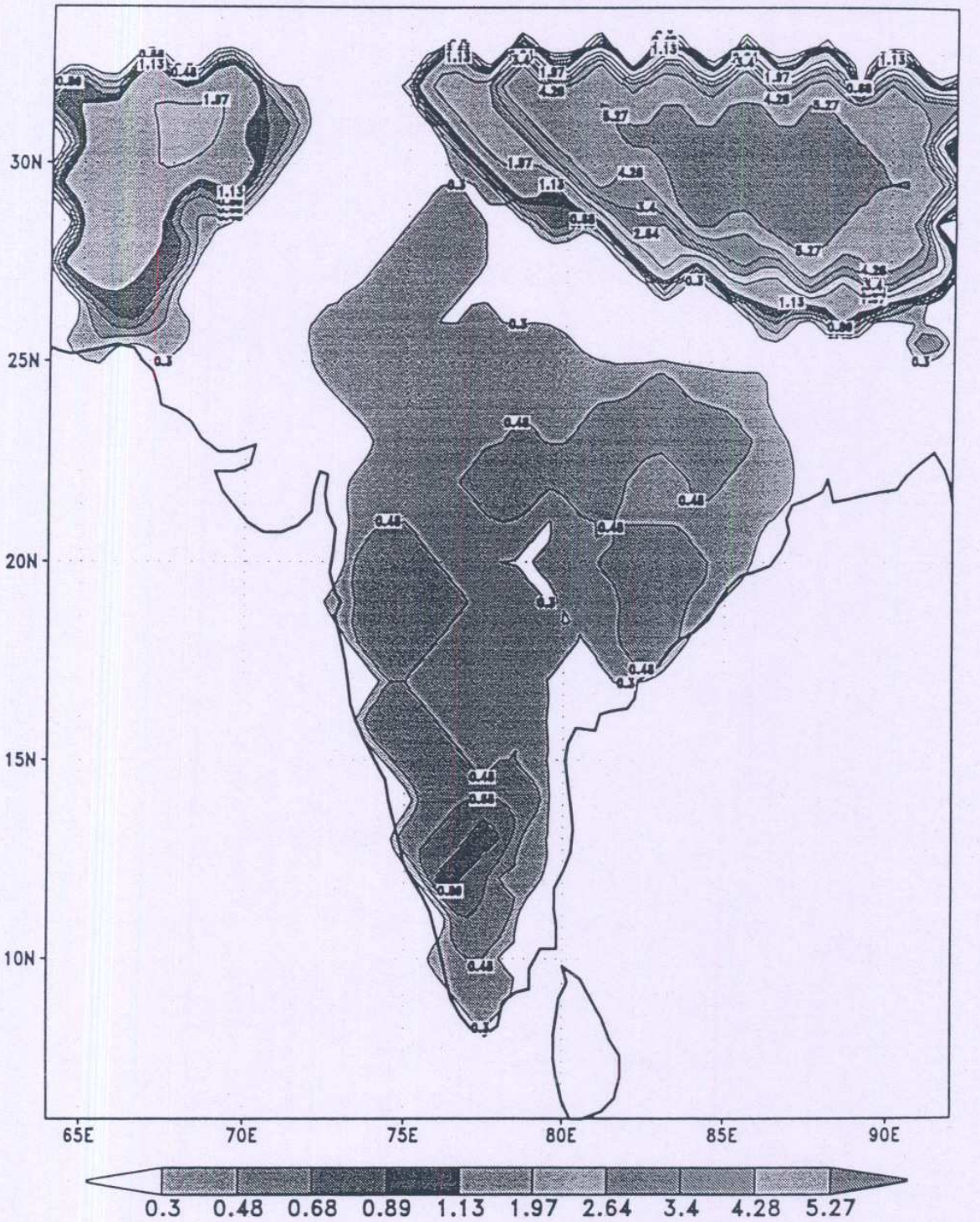

fig 8: Terrain heights used in Eta Model(0.50 Deg). Steps at .3 .48 .68 .89 1.13 1.97 2.64 3.40 4.28 5.27 km are shown with contours.

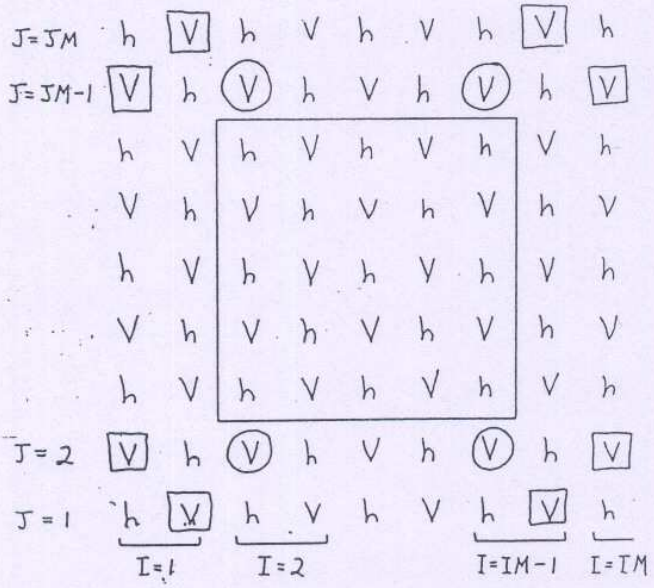

fig 9 The eta model E grid with solid line enclosing the integration domain. Boxed and circled V are handeled differently in boundary region (Black, 1988)

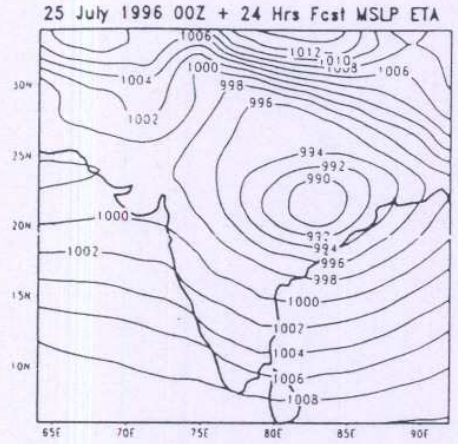

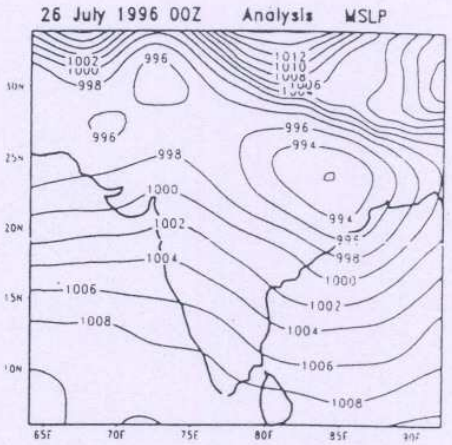

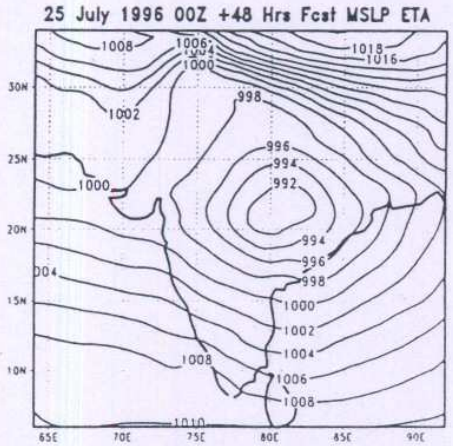

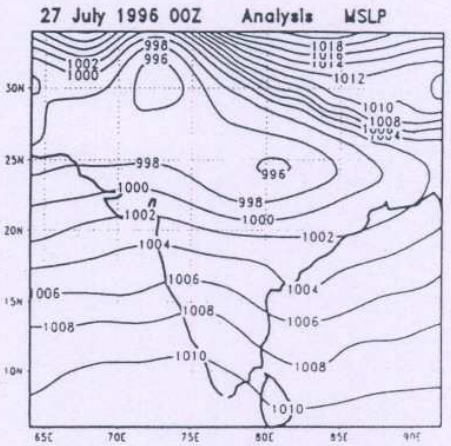

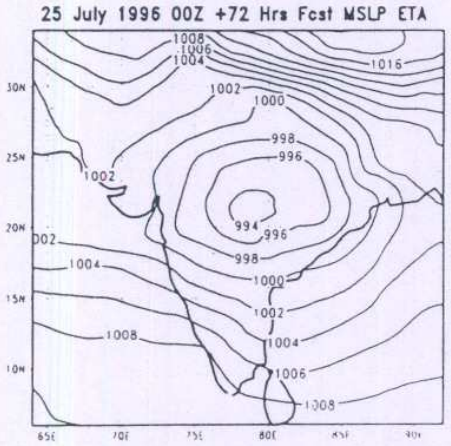

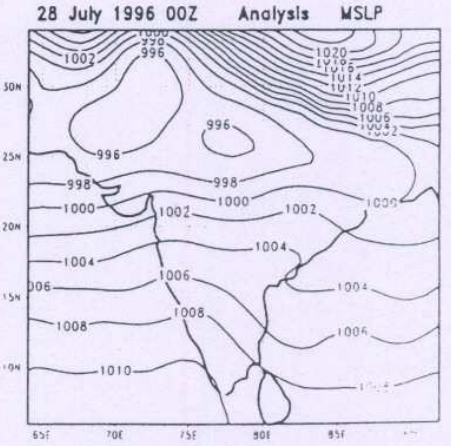

Fig 10: ETA model(0.5 deg.) Forecast and Analysis of Mean sea level pressure (hPa)

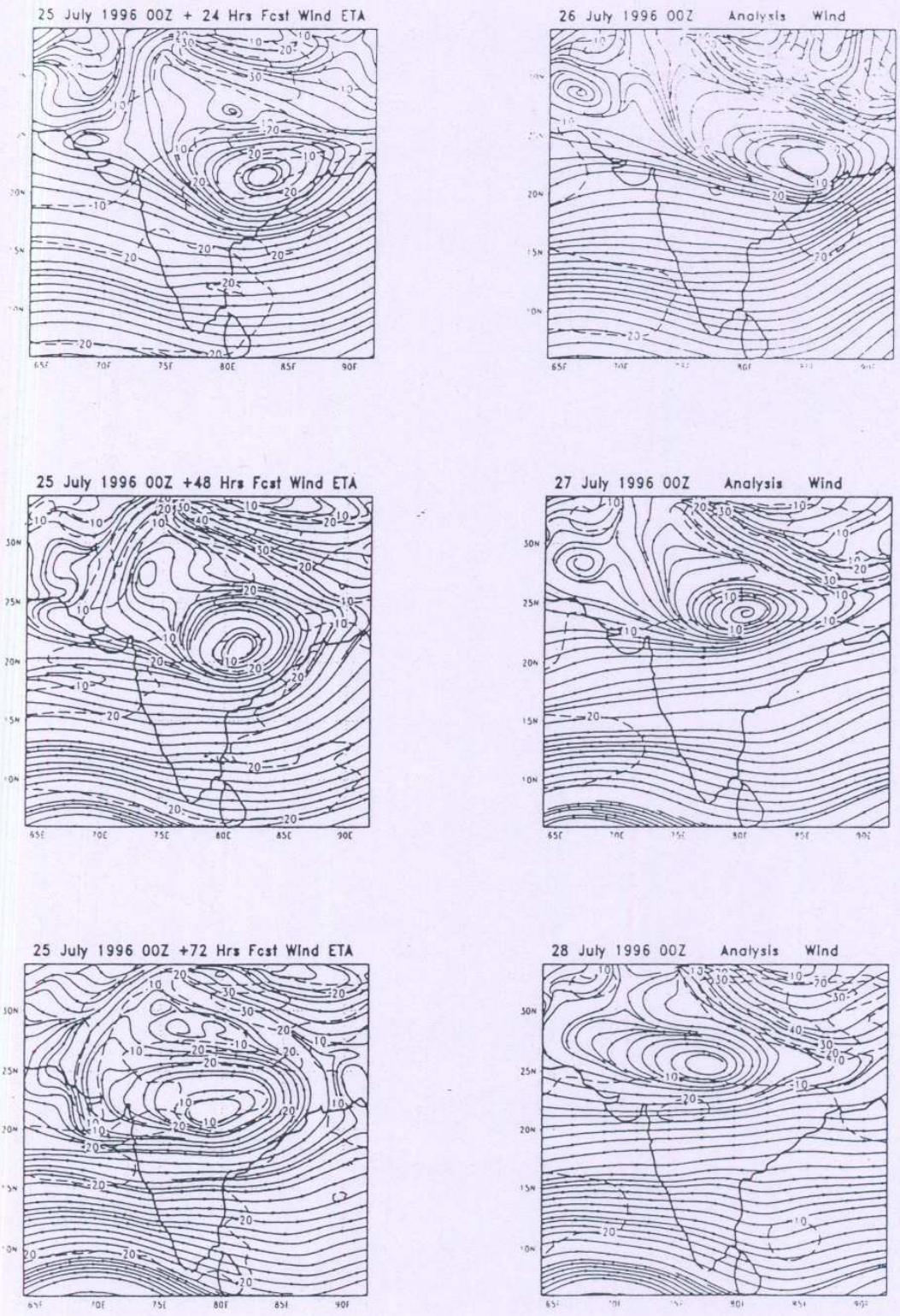

Fig 11: ETA model(0.5 deg.) Forecast and Analysis of Streamlines & isotachs(m/s) at 850 hPa

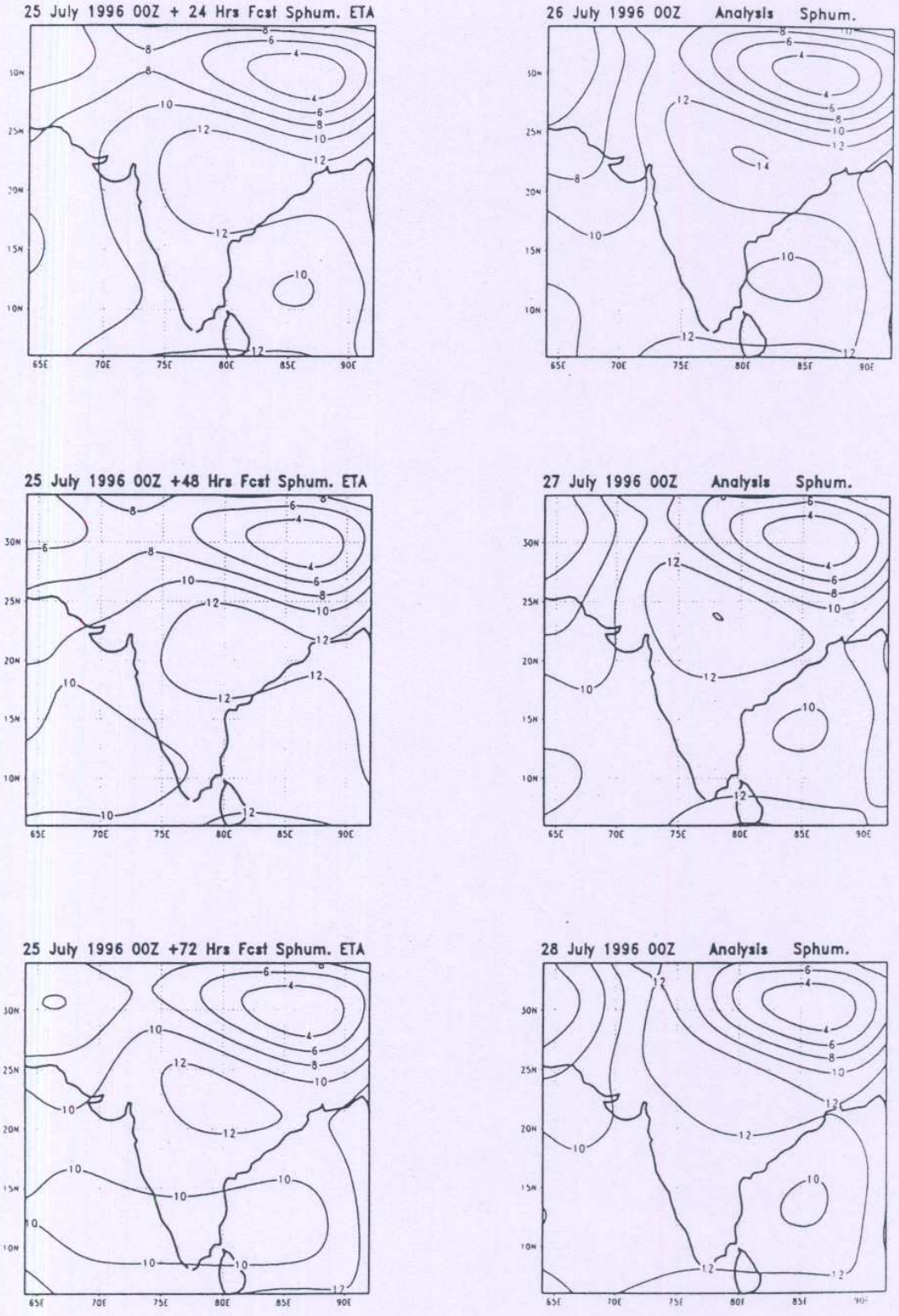

Fig 12: ETA model(0.5 deg.) Forecast and Analysis of Specific humidity(gm/Kg) at 850 hPa

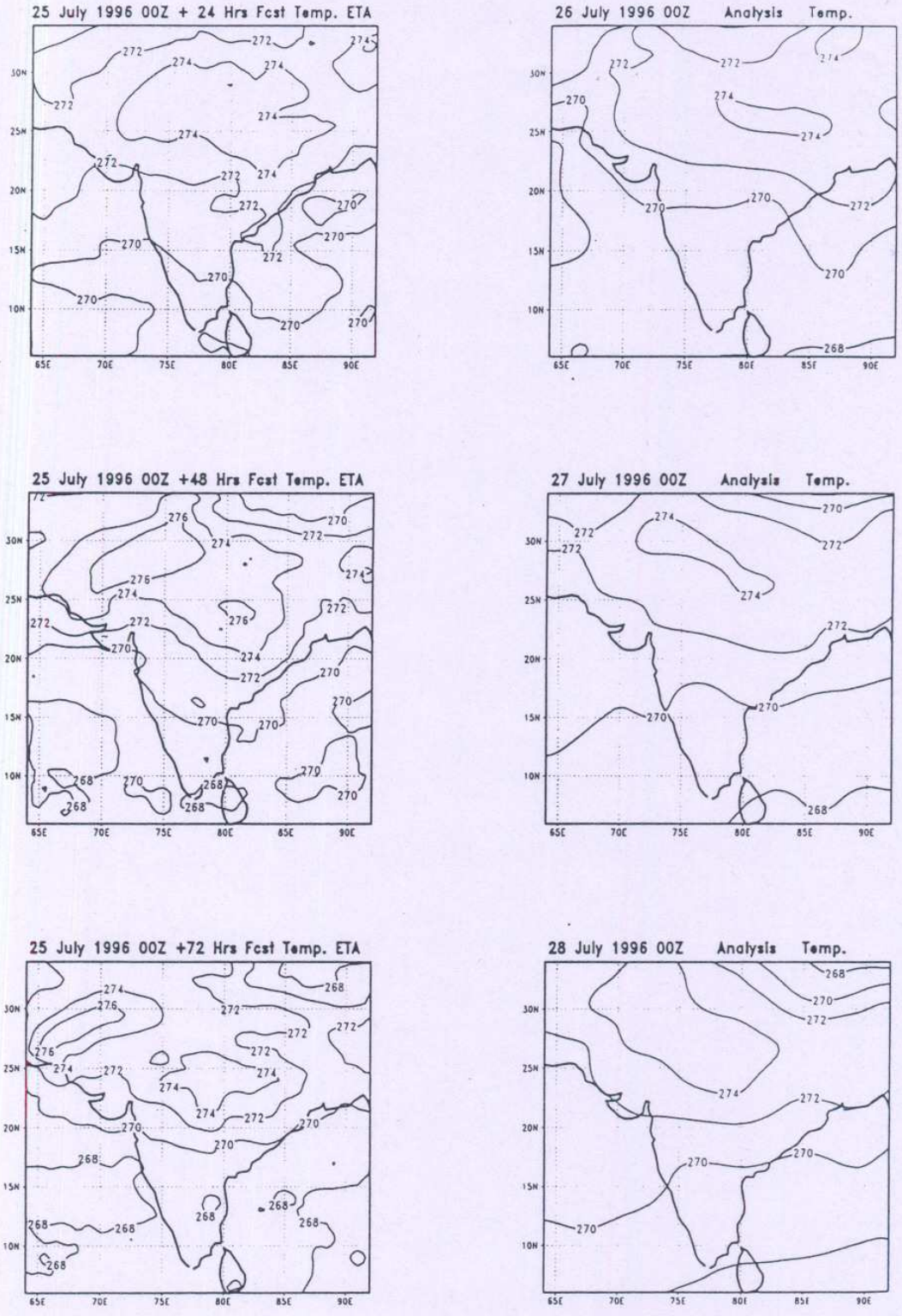

Fig 13: ETA model(0.5 deg.) Forecast and Analysis of Temperature(K) at 500 hPa

Input 25 July 1996 00Z +24 Hr Rainfall(cm/day)

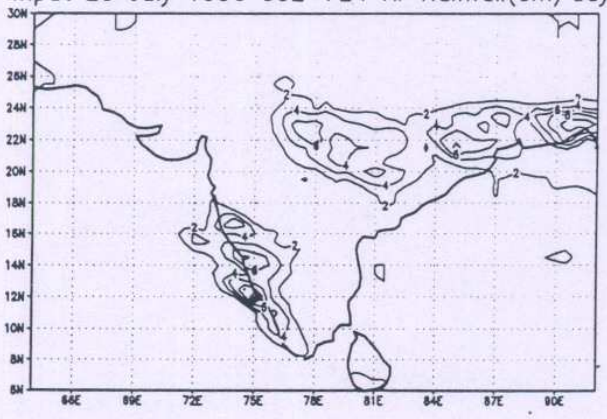

Input 25 July 1996 00Z +48 Hr Rainfall(cm/day)

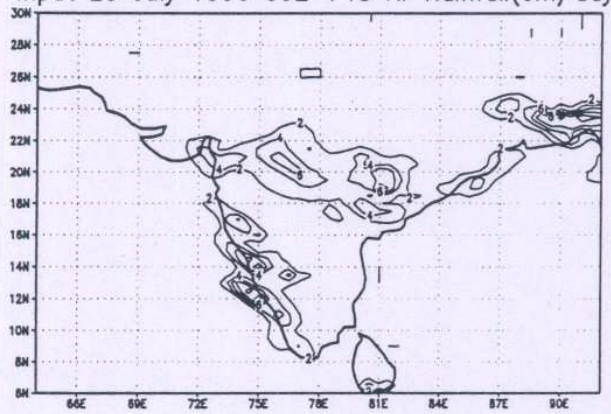

Input 25 July 1996 00Z +72 Hr Rainfall(cm/day)

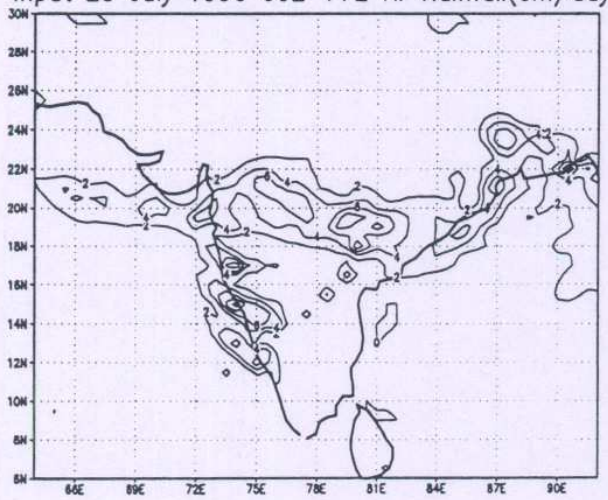

Fig 14: Forecast Rainfall–Eta 0.50 Deg

I. I. T. M. RESEARCH REPORTS

1. Energetic consistency of truncated models, *Asnani G.C.*, August 1971, RR-001.

2. Note on the turbulent fluxes of heat and moisture in the boundary layer over the Arabian Sea, *Sinha S.*, August 1971, RR-002.

3. Simulation of the spectral characteristics of the lower atmosphere by a simple electrical model and using it for prediction, *Sinha S.*, September 1971, RR-003.

4. Study of potential evapo- transpiration over Andhra Pradesh, *Rakhecha P.R.*, September 1971, RR-004.

5. Climatic cycles in India -1 : Rainfall, *Jagannathan P. and Parthasarathy B.*, November 1971, RR-005.

6. Tibetan anticyclone and tropical easterly jet, *Raghavan K.*, September 1972, RR-006.

7. Theoretical study of mountain waves in Assam, *De U.S.*, February 1973, RR-007.

8. Local fallout of radioactive debris from nuclear explosion in a monsoon atmosphere, *Saha K.R. and Sinha S.*, December 1972, RR-008.

9. Mechanism for growth of tropical disturbances, *Asnani G.C. and Keshavamurty R.N.*, April 1973, RR-009.

10. Note on "Applicability of quasi-geostrophic barotropic model in the tropics", *Asnani G.C.*, February 1973, RR-010.

11. On the behaviour of the 24-hour pressure tendency oscillations on the surface of the earth, Part-I: Frequency analysis, Part-II: Spectrum analysis for tropical stations, *Misra B.M.*, December 1973, RR-011.

12. On the behaviour of the 24 hour pressure tendency oscillations on the surface of the earth, Part-III: Spectrum analysis for the extra-tropical stations, *Misra B.M.*, July 1976, RR-011A.

13. Dynamical parameters derived from analytical functions representing Indian monsoon flow, *Awade S.T. and Asnani G.C.*, November 1973, RR-012.

14. Meridional circulation in summer monsoon of Southeast Asia, *Asnani G.C.*, November 1973, RR-014.

15. Energy conversions during weak monsoon, *Keshavamurty R.N. and Awade S.T.*, August 1974, RR-015.

16. Vertical motion in the Indian summer monsoon, *Awade S.T. and Keshavamurty R.N.*, August 1974, RR-016.

17. Semi-annual pressure oscillation from sea level to 100mb in the northern hemisphere, *Asnani G.C. and Verma R..K..*, August 1974, RR-017.

18. Suitable tables for application of gamma probability model to rainfall, *Mooley D.A.*, November 1974, RR-018.

19. Annual and semi-annual thickness oscillation in the northern hemisphere, *Asnani G.C. and Verma R.K.*, January 1975, RR-020.

20. Spherical harmonic analysis of the normal constant pressure charts in the northern hemisphere, *Awade S.T., Asnani G.C. and Keshavamurty R.N.*, May 1978, RR-021.

21. Dynamical parameters derived from analytical function representing normal July zonal flow along 87.5 °E, *Awade S.T. and Asnani G.C.*, May 1978, RR-022.

22. Study of trends and periodicities in the seasonal and annual rainfall of India, *Parthasarathy B. and Dhar O.N.*, July 1975, RR-023.

23. Southern hemisphere influence on Indian rainfall, *Raghavan K.., Paul D.K.. and Upasani P.U.*, February 1976, RR-024.

24. Climatic fluctuations over Indian region - Rainfall : A review, *Parthasarathy B. and Dhar O.N.*, May 1978, RR-025.

25. Annual variation of meridional flux of sensible heat, *Verma R..K. and Asnani G.C.*, December 1978, RR-026.

26. Poisson distribution and years of bad monsoon over India, *Mooley D.A and Parthasarathy B.*, April 1980, RR-027.

27. On accelerating the FFT of Cooley and Tukey, *Mishra S.K.*., February 1981, RR-028.

28. Wind tunnel for simulation studies of the atmospheric boundary layer, *Sivaramakrishnan S.*, February 1981, RR-029.

29. Hundred years of Karnataka rainfall, *Parthasarathy B. and Mooley D.A.*, March 1981, RR-030.

30. Study of the anomalous thermal and wind patterns during early summer season of 1979 over the Afro-Asian region in relation to the large-scale performance of the monsoon over India, *Verma R. K. and Sikka D.R.* , March 1981, RR-031.

31. Some aspects of oceanic ITCZ and its disturbances during the onset and established phase of summer monsoon studied with Monex-79 data, *Sikka D.R., Paul D.K. and Singh S.V.*, March 1981, RR- 032.

32. Modification of palmer drought index, *Bhalme H.N. and Mooley D.A.*, March 1981, RR-033.

33. Meteorological rocket payload for Menaka-II/Rohini 200 and its developmental details, *Vernekar K.G. and Brij Mohan*, April 1981, RR-034.

34. Harmonic analysis of normal pentad rainfall of Indian stations, *Anathakrishnan R. and Pathan J.M.*, October 1981, RR-035.

35. Pentad rainfall charts and space-time variations of rainfall over India and the adjoining areas, *Anathakrishnan R.. and Pathan J.M.*, November 1981, RR-036.

36. Dynamic effects of orography on the large scale motion of the atmosphere Part I : Zonal flow and elliptic barrier with maximum height of one km., *Bavadekar S.N. and Khaladkar R.M.*, January 1983, RR-037.

37. Limited area five level primitive equation model, *Singh S.S.*, February 1983, RR-38.

38. Developmental details of vortex and other aircraft thermometers, *Vernekar K.G., Brij Mohan and Srivastava S.*, November 1983, RR-039.

39. Note on the preliminary results of integration of a five level P.E. model with westerly wind and low orography, *Bavadekar S.N., Khaladkar R.M., Bandyopadhyay A. and Seetaramayya P.*, November 1983, RR-040.

40. Long-term variability of summer monsoon and climatic change, *Verma R.K., Subramaniam K. and Dugam S.S.*, December 1984, RR-041.

41. Project report on multidimensional initialization for NWP models, *Sinha S.*, February 1989, RR-042.

42. Numerical experiments with inclusion of orography in five level P.E. Model in pressure-coordinates for interhemispheric region, *Bavadekar S.N. and Khaladkar R.M.*, March 1989, RR-043.

43. Application of a quasi-lagrangian regional model for monsoon prediction, *Singh S.S. and Bandyopadhyay A.*, July 1990, RR-044.

44. High resolution UV-visible spectrometer for atmospheric studies, *Bose S., Trimbake H.N., Londhe A.L. and Jadhav D.B.*, January 1991, RR-045.

45. Fortran-77 algorithm for cubic spline interpolation for regular and irregular grids, *Tandon M.K.*, November 1991, RR-046.

46. Fortran algorithm for 2-dimensional harmonic analysis, *Tandon M.K.*, November 1991, RR- 047.

47. 500 hPa ridge and Indian summer monsoon rainfall : A detailed diagnostic study, *Krishna Kumar K., Rupa Kumar K. and Pant G.B.*, November 1991, RR-048.

48. Documentation of the regional six level primitive equation model, *Singh S.S. and Vaidya S.S.*, February 1992, RR-049.

49. Utilisation of magnetic tapes on ND-560 computer system, *Kripalani R.H. and Athale S.U.*, July 1992, RR-050.

50. Spatial patterns of Indian summer monsoon rainfall for the period 1871-1990, *Kripalani R.H., Kulkarni A.A., Panchawagh N.V. and Singh S.V.*, August 1992, RR-051.

51. FORTRAN algorithm for divergent and rotational wind fields, *Tandon M.K.*, November 1992, RR-052.

52. Construction and analysis of all-India summer monsoon rainfall series for the longest instrumental period : 1813-1991., *Sontakke N.A., Pant G.B. and Singh N.*, October 1992, RR-053.

53. Some aspects of solar radiation, *Tandon M.K.*, February 1993, RR-054.

54. Design of a stepper motor driver circuit for use in the moving platform, *Dharmaraj T. and Vernekar K.G.*, July 1993, RR-055.

55. Experimental set-up to estimate the heat budget near the land surface interface, *Vernekar K.G., Saxena S., Pillai J.S., Murthy B.S., Dharmaraj T. and Brij Mohan*, July 1993, RR-056.

56. Identification of self-organized criticality in atmospheric total ozone variability, *Selvam A.M. and Radhamani M.*, July 1993, RR-057.

57. Deterministic chaos and numerical weather prediction, *Selvam A.M.*, February 1994, RR-058.

58. Evaluation of a limited area model forecasts, *Singh S.S., Vaidya S.S, Bandyopadhyay A., Kulkarni A.A, Bawiskar S.M., Sanjay J., Trivedi D.K.and Iyer U.*, October 1994, RR-059.

59. Signatures of a universal spectrum for atmospheric interannual variability in COADS temperature time series, *Selvam A.M., Joshi R.R. and Vijayakumar R.*, October 1994, RR-060.

60. Identification of self-organized criticality in the interannual veriability of global surface temperature, *Selvam A.M. and Radhamani M.*, October 1994, RR-061.

61. Identification of a universal spectrum for nonlinear veriability of solar-geophysical parameters, *Selvam A.M., Kulkarni M.K., Pethkar J.S. and Vijayakumar R.*, October 1994, RR-062.

62. Universal spectrum for fluxes of energetic charged particles from the earth's magnetosphere, *Selvam A.M. and Radhamani M.*, June 1995, RR-063.

63. Estimation of nonlinear kinetic energy exchanges into individual triad interactions in the frequency domain by use of the cross-spectral technique, *Chakraborty D.R.*, August 1995, RR-064.

64. Monthly and seasonal rainfall series for all-India homogeneous regions and meteorological subdivisions : 1871-1994, *Parthasarathy B., Munot A.A. and Kothawale D.R.*, August 1995, RR-065.

65. Thermodynamics of the mixing processes in the atmospheric boundary layer over Pune during summer monsoon season, *Morwal S.B. and Parasnis S.S.*, March 1996, RR-066.

66. Instrumental period rainfall series of the Indian region : A documentation, *Singh N. and Sontakke N.A.*, March 1996, RR-067.

67. Some numerical experiments on roundoff-error growth in finite precision numerical computation, *Fadnavis S.*, May 1996, RR-068.

68. Fractal nature of MONTBLEX time series data, *Selvam A.M. and Sapre V.V.*, May 1996, RR-069.

69. Homogeneous regional summer monsoon rainfall over India : Interannual variability and teleconnections, *Parthasarathy B., Rupa Kumar K. and Munot A.A.*, May 1996, RR-070.

70. Universal spectrum for sunspot number variability, *Selvam A.M. and Radhamani M.*, November 1996, RR-071.

71. Development of simple reduced gravity ocean model for the study of upper north Indian ocean, *Behera S.K. and Salvekar P.S.*, November 1996, RR-072.

72. Study of circadian rhythm and meteorological factors influencing acute myocardial infraction, *Selvam A.M., Sen D. and Mody S.M.S.*, April 1997, RR-073.

73. Signatures of universal spectrum for atmospheric gravity waves in southern oscillation index time series, *Selvam A.M., Kulkarni M.K., Pethkar J.S. and Vijayakumar R.*, December 1997, RR-074.

74. Some example of X-Y plots on Silicon Graphics, *Selvam A.M., Fadnavis S. and Gharge S.P.*, May 1998, RR-075.

75. Simulation of monsoon transient disturbances in a GCM, *Ashok K., Soman M.K. and Satyan V.*,August 1998, RR-076.

76. Universal spectrum for intraseasonal variability in TOGA temperature time series, *Selvam A.M., Radhamani M., Fadnavis S. and Tinmaker M.I.R.*, August 1998, RR-077.

77. One dimensional model of atmospheric boundary layer, *Parasnis S.S., Kulkarni M.K., Arulraj S. and Vernekar K.G.*, February 1999, RR-078.

78. Diagnostic model of the surface boundary layer - A new approach, *Sinha S.*, February 1999, RR-079.

79. Computation of thermal properties of surface soil from energy balance equation using force - restore method, *Sinha S.*, February 1999, RR-080.

80. Fractal nature of TOGA temperature time series, *Selvam A.M. and Sapre V.V.*, February 1999, RR-081.

81. Evolution of convective boundary layer over the Deccan Plateau during summer monsoon, *Parasnis S.S.*, February 1999, RR-082.

82. Self - organized criticality in daily incidence of acute myocardial infarction, *Selvam A.M., Sen D., and Mody S.M.S.*, Feburary 1999, RR-083.

83. Monsoon simulation of 1991 and 1994 by GCM : Sensitivity to SST distribution, *Ashrit R.G., Mandke S.K. and Soman M.K.*, March 1999, RR-084.

84. Numerical investigation on wind induced interannual variability of the north Indian Ocean SST, Behera S.K., Salvekar P.S. and Ganer D.W., April 1999, RR-085.

.. ..